THE JOURNAL OF PHYSICAL CHEMISTRY C

Article

Cite This: J. Phys. Chem. C 2019, 123, 1021−1031

pubs.acs.org/JPCC

Mean First-Passage Time and Steady-State Transfer Rate in Classical Chains

Published as part of The Journal of Physical Chemistry virtual special issue "Abraham Nitzan Festschrift".

Na'im Kalantar and Dvira Segal*

Department of Chemistry and Centre for Quantum Information and Quantum Control, University of Toronto, 80 Saint George Street, Toronto, Ontario M5S 3H6, Canada

Supporting Information

ABSTRACT: Understanding excitation and charge transfer in disordered media is a significant challenge in chemistry, biophysics, and material science. We study two experimentally relevant measures for carrier transfer in finite-size chains, a mean first-passage time (MFPT) and the steady-state transfer time (SSTT). We discuss the relationship between these measures and derive analytic formulas for 1D chains. We exemplify the behavior of these time scales in different motifs: donor−bridge−acceptor systems, biased chains, and alternating and stacked copolymers. We find that the MFPT and the SSTT may administer different, complementary information on the system, jointly reporting on molecular length and energetics. Under constraints such as fixed donor−acceptor energy bias, we show that the MFPT and the SSTT are optimized (minimized) under fundamentally different internal potential profiles. This study brings insights into the behavior of the MFPT and the SSTT and suggests that it is beneficial to perform both transient and steady-state measurements on a conducing network so as to gather a more complete picture of its properties.

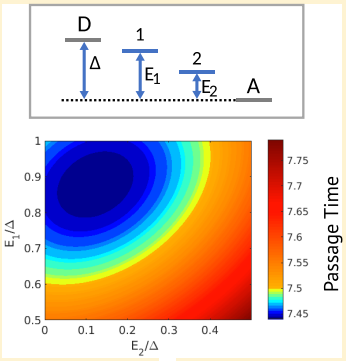

1. INTRODUCTION

Understanding charge- and energy-transfer processes in soft and disordered materials such as thin films made from organic polymers or large biological molecules is central to the development of electronic and energy solar-harvesting applications.[1] To model such systems efficiently, a coarse-grained model of the surrounding environment is often assumed. In turn, this approach allows the application of kinetic, Markovian master equations for following the dynamics of averaged variables.

Mean first-passage quantities are useful for characterizing stochastic processes. Specifically, the mean first-passage time defines a time scale to visit a specified target (or a threshold value) for the first time.[2] This measure finds numerous applications in physics, chemistry, and biology, for example, for quantifying reaction rates, transmission of particles in channels, molecular processes such as receptor binding and adhesion, and cellular processes such as cell division.[3] Here we focus on (charge or energy) transfer processes in flexible molecular systems and use the mean first-passage time to report on the transfer process from a certain initial site to a final location.[4]

The capacity of molecules to transfer electric charge can be measured in different setups. In transient absorption spectroscopy experiments, an initial state is carefully prepared and monitored in time; see, for example, refs 5−7. In contrast, in electrochemical experiments, a molecule of interest is attached to an electrode, and the rate of charge transfer from the electrode to redox groups in the molecule is monitored; see, for example, ref 8. Alternatively, in molecular conductance experiments, a molecule links two voltage-biased electrodes, for example, an STM tip and a conducting substrate, and the molecule is characterized by its electrical conductance.[9] To thoroughly understand charge-transfer processes in a single molecule or ensemble of molecules, it is critical to resolve the connection between measured observables in such different experiments. A somewhat related problem was recently explored in ref 10, checking the relation between optoelectronic properties of semiconductors deduced from either pulsed excitation methods or steady-state measurements.

Several theoretical studies predicted a linear relationship between the intramolecular charge-transfer rate in a donor−bridge−acceptor system and the low bias conductance in a metal−molecule−metal junction.[11−15] Nevertheless, experiments revealed a more complex behavior.[8,16,17] For example, in ref 8, the electrochemical rate constant and the molecular conductance were examined in alkane chains and peptide nucleic acid oligomers, generally manifesting nonlinear correlations between the transfer rate and the conductance. These deviations from linearity are rationalized by noting that for the same molecule, transient, electrochemical, and conductance measurements are performed at undoubtedly different settings, considering ensemble versus single molecule,

Received: September 11, 2018
Revised: December 9, 2018
Published: December 10, 2018

DOI: 10.1021/acs.jpcc.8b08874
J. Phys. Chem. C 2019, 123, 1021−1031

using different solvents, and experiencing different environmental conditions. As a result, the energetics of the molecule and its dephasing and relaxation processes are different in the these distinct types of experiments.

In this work, we revisit the following basic question: Considering carrier transfer processes in 1D hopping systems, what is the relationship between transient measures and steady-state observables? We leave aside the challenging, practical problem discussed above, that in different experimental settings the molecule and its local environment are modified, and, for simplicity, we assume that the structures are identical in the different types of experiments.

Using classical rate equations, we compare transient and steady-state measures for the transfer process, namely, a mean first-passage time (MFPT) and the inverse of the steady-state rate, referred to as the steady-state transfer time (SSTT). On the basis of these two measures, we study the roles of structural motifs on carrier transfer in different networks, including linear or branched chains and uniform, bridge-mediated, energy-biased, single, and multicomponent networks. We derive a simple, intuitive relationship between the two time scales, the MFPT and the SSTT, and explain under what conditions they agree. In general, we find that these measures scale differently with system size and energy and that they can disclose distinct properties of the system. We further discuss the enhancement of the transfer speed by optimizing the energy profile of the system, achieved, for example, by chemical modifications or gating.

2. MODEL AND MEASURES

We study the problem of a random walk across a finite system. The model includes $n + 2$ sites, with a donor D (site 0), acceptor A (site $n + 1$), and n intermediate sites. We use the chemistry notation of donor and acceptor to identify the edges of the chain. In addition, the model includes a trap T attached only to A; transitions from A to the trap are irreversible, with a trapping rate constant Γ_A. Variants of this model have been adopted to describe the charge transfer and excitation energy transport in polymers, biomolecules, and amorphous systems. A model with multiple acceptors is discussed in the Supporting Information. At this point, we do not specify the connectivity or the energy profile of the system, to be described in examples. Also, we do not include lossy processes within the system, such as exciton recombination.

The Pauli master equation describes the time evolution of site populations, p_i, $i = 0, 1, ..., n + 1$

$$\dot{\mathbf{p}}(t) = \mathbf{M}\mathbf{p}(t) \tag{1}$$

with the vector of population $\mathbf{p}$ and rate constant matrix $\mathbf{M}$. Note that this system of equations does not include the equation of motion for the trap, which fulfills $\dot{p}_T = \Gamma_A p_A$. In such a coarse-grained random walk model, the properties of the environment, such as its temperature, determine the hopping rates; to make a transition up (down) in energy, the walker absorbs (dissipates) heat from (to) the surrounding thermal bath. The differential equation (eq 1) is linear and first-order and therefore can be readily solved. We particularly mention that in many instances experiments of charge transfer in DNA are well described by the Pauli rate equations; see, for example, refs 18−23.

The success rate of a transfer process in a kinetic network can be quantified using different measures, such as the transfer time, yield, and flux. Before we introduce the different observables, we present time-dependent and steady-state experiments. In the first case, realized, for example, with transient absorption spectroscopy, one prepares a well-defined initial condition and follows the time evolution of the system toward its long-time state. For example, in studies of charge transfer in DNA, an excess charge is prepared on a donor site using a laser excitation. Once injected into the DNA, the excess charge migrates until it arrives at an acceptor molecule attached to the DNA.[5−7] Mathematically, transient dynamics is revealed by solving the time-dependent, first-order differential eq 1. The formal solution is $\mathbf{p}(t) = \exp(\mathbf{M}t)\mathbf{p}_0$, with the vector of the initial condition $\mathbf{p}_0$.

Alternatively, one may study the same system, albeit in a steady-state situation, by defining a boundary condition rather than an initial condition, identifying a source and a sink (possibly more than one). For example, the donor population can be maintained fixed by continuously feeding in particles; population leaves the acceptor at the same rate. In this scenario, the relevant measure for the transfer process is the flux of outgoing particles, from the acceptor—outside. As was discussed in, for example, refs 11−15, in a donor−bridge−acceptor configuration and under some simplifying assumptions, this steady-state setup can be furthermore related to the low-voltage electrical conductance.

In what follows, we consider time-dependent and steady-state settings, examine transfer measures, and discuss their relationships. We emphasize that we focus here on systems that include a single donor and a single acceptor and that so far we do not consider losses within the network.

2.1. Mean First-Passage Time. The mean first-passage time defines a time scale for a random event to occur for the first time. A trapping time scale describes the mean time it takes for population to leave the system, that is, to transfer from the donor to the trap. Let us consider our model, with $n + 2$ sites and a trap. From the conservation of population, $1 = \sum_{i=0}^{n+1} p_i + p_T$. Here $p_T(t)$ is the trap population and $\dot{p}_T(t)$ is the instantaneous trapping rate. This quantity is normalized, $\int_0^\infty \dot{p}_T(t)\, dt = 1$; therefore, it represents the probably density of trapping time, t. We can now define the mean trapping time, referred to as the trapping mean first-passage time, by

$$\tau_m \equiv \int_0^\infty t\dot{p}_T(t)\, dt \tag{2}$$

See also ref 24. Because the probability of not having transitioned to the trap is equal to the probability of being in the other $n + 2$ sites of the system, $\dot{p}_T(t) = -\sum_{j=0}^{n+1} \dot{p}_j(t)$. Integrating by parts, we get

$$\tau_m = \sum_{j=0}^{n+1} \int_0^\infty p_j(t)\, dt = \sum_{j=0}^{n+1} r_j \tag{3}$$

where the residence time on the jth site is defined as

$$r_j \equiv \left[\int_0^\infty \exp(\mathbf{M}t)\mathbf{p}_0\, dt\right]_j = [-\mathbf{M}^{-1}\mathbf{p}_0]_j \tag{4}$$

Note that we count rows starting from 0 to $n + 1$. Alternatively, the MFPT can be calculated from the accumulated population on the acceptor; the rate equation describing the kinetics of the trap fulfills $\dot{p}_T(t) = \Gamma_A p_A(t)$; therefore

DOI: 10.1021/acs.jpcc.8b08874
J. Phys. Chem. C 2019, 123, 1021−1031

$$\tau_m = \Gamma_A \int_0^\infty t p_A(t)\, dt \tag{5}$$

Equations 3 and 5 are equivalent; computationally, the former is more convenient. We emphasize that the MFPT, as well as other observables considered below, are calculated without the explicit consideration of the trap population.

Another method to calculate the MFPT is to replace the trap and the donor states with a combined donor/trap state. The steady state for this configuration gives the MFPT by

$$\frac{1}{\tau_m} = \Gamma_A p_{D/T} \tag{6}$$

where $p_{D/T}$ is the steady-state population of the combined donor/trap state. This scheme allows the calculation of MFPT for systems with a backflow from the trap state to the acceptor.[25] In the rest of the paper, we calculate the MFPT based on eqs 3 and 4.

2.2. Mean-Transfer Time. Another measure that has been commonly introduced in the literature is the average transfer time to reach the acceptor, written as

$$\tau_t \equiv \frac{\int_0^\infty t p_A(t)\, dt}{\int_0^\infty p_A(t)\, dt} \tag{7}$$

Nevertheless, because $\int_0^\infty \Gamma_A p_A(t) dt = \int_0^\infty \dot{p}_T(t) dt = 1$, eq 7 is identical to eq 5, and we conclude that the MFPT and the mean-transfer time are in fact the same measure. Note that these considerations hold even if the underlying dynamics involves nonthermal effects or quantum effects comprising the time evolution of coherences.

2.3. Steady-State Flux. In a steady-state experiment we maintain the population of the donor state fixed, $p_D(t) = 1$, and measure the outgoing particle flux from the acceptor toward the trap. In the long time limit, transient effects die out, $\dot{\mathbf{p}}(t) = 0$. The differential equation reduces to an algebraic one for the population. There are different equivalent ways to organize the algebraic equation for the population, as we discuss in the Supporting Information, Section S1. Here we solve

$$\tilde{\mathbf{M}}\mathbf{p}_{ss} = \mathbf{v} \tag{8}$$

where $\tilde{\mathbf{M}}$ corresponds to the matrix $\mathbf{M}$ of eq 1 by replacing its first row by (1 0 0 ...). The inhomogeneous column $\mathbf{v}$ has a single nonzero value (unity) in its first element, $\mathbf{v} = (1\ 0\ 0\ ...)^T$. The first row of eq 8 thus stands for the condition $p_D^{ss} = 1$, that is, the donor-state population in steady state. We exemplify these definitions in the Supporting Information (Section S1). We solve eq 8 and obtain the steady-state population. The steady-state flux is defined as

$$k_{ss} \equiv \Gamma_A p_A^{ss} / p_D^{ss} \tag{9}$$

but we can omit the denominator, which was written here to highlight the normalization with respect to the donor occupation. The inverse of the flux defines a time scale

$$\tau_{ss} \equiv k_{ss}^{-1} \tag{10}$$

which we refer to as the "steady-state transfer time".

2.4. On the Relation between the MFPT and the Steady-State Flux. Because different protocols (transient and steady state) may be used to interrogate the same system, it is critical to resolve the relationship between the MFPT and the SSTT. Do these measures necessarily convey the same information? If not, when do these time scales agree? This question will be discussed throughout the paper: We provide examples in which the two measures, eqs 3 and 10, converge and situations in which they report on different properties of the system.

Intuitively, as was for example explained in refs 26 and 27, the MFPT and the SSTT agree when the dynamics is dominated by a single decaying exponent. Considering the eigenvalues of the kinetic matrix $\mathbf{M}$; this situation manifests itself when $|(\lambda_1 - \lambda_0)/\lambda_0| \gg 1$. Here λ_0 is the smallest (in magnitude) eigenvalue of $\mathbf{M}$, and λ_1 is the next eigenvalue in order of increasing magnitude. Whereas mathematically, this condition is clear, its physical implications are not transparent.

What physical picture can assist us in understanding the agreement between or the divergence of these two measures? As we now show, we can derive a simple relationship between these two measures with very little effort. In the steady state, the outgoing flux is equal to the incoming flux, and thus we write down the following relation (see the Supporting Information)

$$\mathbf{M}\mathbf{p}^{ss} = (-k_{ss}\ \ 0\ \ 0\ \ ...)^T = -k_{ss}\mathbf{p}_0 \tag{11}$$

Here $\mathbf{p}^{ss}$ is the vector of population in the steady state. The second equality in eq 11 relies on the initial condition assumed in the transient problem (only the donor site is occupied), and we therefore replaced the unit vector $(1\ 0\ 0\ ...)^T$ by the vector of initial condition, $\mathbf{p}_0$. We now use eq 4 and find that

$$\mathbf{p}^{ss} = k_{ss}\mathbf{r} \tag{12}$$

On the left-hand side we have a vector of steady-state population. On the right-hand side, $\mathbf{r}$ is the vector of residence times. Summing up the rows and using eq 3, where we identify the sum of the residence times by the MFPT, we get

$$\sum_{j=0}^{n+1} [p^{ss}]_j = k_{ss}\tau_m \tag{13}$$

or

$$p_{total}^{ss} = \tau_m/\tau_{ss} \tag{14}$$

Here we define the total population as p_{total}^{ss}, including donor, n intermediate sites, and acceptor. Equation 14 is deceitfully simple yet powerful, and it is one of the central results of our work. This relation tells us that the transient measure, which is the MFPT, and the steady-state transfer time agree when the total population in the steady-state problem sums up to 1. Of course, because we set the steady-state boundary condition by fixing $p_D^{ss} = 1$, the total population in the steady state is always greater than 1, and the two measures always disagree to some extent. However, we can now predict based on physical intuition whether this deviation is large or small.

The first critical observation from eq 14 is that when we measure a certain system with transient and steady-state methods, we should always find that $\tau_m > \tau_{ss}$. If we violate this inequality, then we obviously suffer from a critical problem; for example, the physical structure is not the same in the two experiments, possibly due to modifications to the surrounding environment.

Let us now consider a three-site (D,1,A) donor–bridge–acceptor model. The total occupation of the system is

DOI: 10.1021/acs.jpcc.8b08874
J. Phys. Chem. C 2019, 123, 1021−1031

$p^{ss}_{total} = p^{ss}_D + p^{ss}_1 + p^{ss}_A$, and obviously, it is >1 (remember that $p^{ss}_D = 1$). However, if the bridge energy is set high relative to the thermal energy, then we expect that $p^{ss}_1 + p^{ss}_A \ll 1$, and thus $\tau_m \approx \tau_{ss}$. This prediction is verified in Section 3.3. In contrast, if the energy profile is uniform, then we expect comparable occupations, $p^{ss}_1, p^{ss}_A \approx p^{ss}_D$, and thus the two time scales diverge. Specifically, for a uniform system with n sites, we estimate equal population all through, and thus $\tau_m \approx n\tau_{ss}$. We derive this result in a rigorous manner in Section 3.3. Furthermore, the two time scales should significantly deviate under a forward bias (when the donor site is placed above the acceptor), but they would agree under a reversed bias, as we show in Section 3.4.

It is important to note that eq 14 is quite general: It does not rely on the details of the network; that is, the model may include transitions beyond nearest neighbors, loops, and so on.

3. ONE-DIMENSIONAL CHAINS WITH ARBITRARY RATES: ANALYTIC RESULTS AND EXAMPLES

In this section, we derive analytical expressions for the MFPT and the SSTT in a nearest-neighbor 1D model. We then exemplify these measures in problems that are interesting in the context of charge and excitation transfer in molecular chains and junctions such as organic polymers and DNA.

The model includes a single donor, n intermediate sites on a chain, an acceptor, and a trap. We calculate the MFPT and the SSTT, discuss their relationship, and exemplify that they may convey distinct, complementary information. Our analytical expression for the MFPT agrees with a previous work.[4] Nevertheless, our simple derivation and the associated analysis of the SSTT provide new physical insights. The population equations of motion satisfy (i = 1, 2, ..., n)

$$\begin{aligned}
\dot{p}_0(t) &= -\overrightarrow{k}_1 p_0(t) + \overleftarrow{k}_0 p_1(t)\\
\dot{p}_i(t) &= -(\overrightarrow{k_{i+1}} + \overleftarrow{k_{i-1}})p_i(t) + \overleftarrow{k}_i p_{i+1}(t) + \overrightarrow{k}_i p_{i-1}(t)\\
\dot{p}_{n+1}(t) &= -(\overleftarrow{k}_n + \Gamma_A)p_{n+1}(t) + \overrightarrow{k_{n+1}} p_n(t)
\end{aligned} \tag{15}$$

with $\overleftarrow{k}_i$ ($\overrightarrow{k}_i$) as the rate constant to make a transition toward site i, which is at the left (right) of the current site. For example, assuming an equilibrium bath at temperature T, the rate constants satisfy the detailed balance relation, $\frac{\overrightarrow{k_{i+1}}}{\overleftarrow{k_i}} = e^{-(E_{i+1}-E_i)/T}$; we set the Boltzmann constant as $k_B \equiv 1$. Nevertheless, our general results in this section do not rely on this particular choice for the rates.

3.1. MFPT. The rate matrix (eq 15) of dimension $(n+2)\times(n+2)$ is tridiagonal (all missing entries are zero)

$$\mathbf{M} = \begin{pmatrix}
-\overrightarrow{k}_1 & \overleftarrow{k}_0 & & & & \\
\overrightarrow{k}_1 & -\overleftarrow{k}_0 - \overrightarrow{k}_2 & \overleftarrow{k}_1 & & 0 & \\
 & \overrightarrow{k}_2 & -\overleftarrow{k}_1 - \overrightarrow{k}_3 & \ddots & & \\
 & & \overrightarrow{k}_3 & \ddots & \overleftarrow{k_{n-1}} & \\
 & 0 & & \ddots & -\overleftarrow{k_{n-1}} - \overrightarrow{k_{n+1}} & \overleftarrow{k}_n \\
 & & & & \overrightarrow{k_{n+1}} & -\overleftarrow{k}_n - \Gamma_A
\end{pmatrix} \tag{16}$$

Our objective is to find the residence times using eq 4, $-\mathbf{M}(\mathbf{r}) = \mathbf{p}_0$. Because $\mathbf{M}$ is tridiagonal, by following the Thomas algorithm,[28] we reduce the above equation to

$$\begin{pmatrix}
1 & -\frac{\overleftarrow{k}_0}{\overrightarrow{k}_1} & & & 0 \\
 & 1 & -\frac{\overleftarrow{k}_1}{\overrightarrow{k}_2} & & \\
 & & 1 & \ddots & \\
 & & & \ddots & -\frac{\overleftarrow{k}_n}{\overrightarrow{k_{n+1}}} \\
0 & & & & 1
\end{pmatrix}(\mathbf{r}) = \begin{pmatrix}
\overrightarrow{k}_1^{-1} \\
\overrightarrow{k}_2^{-1} \\
\overrightarrow{k}_3^{-1} \\
\vdots \\
\overrightarrow{k_{n+1}}^{-1} \\
\Gamma_A^{-1}
\end{pmatrix} \tag{17}$$

The transfer times r_j are obtained by progressing recursively from the last row to the first row

$$\mathbf{r} = \begin{pmatrix}
\frac{1}{\overrightarrow{k}_1}(1 + \overleftarrow{k}_0 r_1) \\
\frac{1}{\overrightarrow{k}_2}(1 + \overleftarrow{k}_1 r_2) \\
\frac{1}{\overrightarrow{k}_3}(1 + \overleftarrow{k}_2 r_3) \\
\vdots \\
\frac{1}{\overrightarrow{k_{n+1}}}(1 + \overleftarrow{k}_n r_{n+1}) \\
\frac{1}{\Gamma_A}
\end{pmatrix} \tag{18}$$

or explicitly

$$\mathbf{r} = \begin{pmatrix}
\frac{1}{\overrightarrow{k}_1}\left(1 + \frac{\overleftarrow{k}_0}{\overrightarrow{k}_2}\left(1 + \frac{\overleftarrow{k}_1}{\overrightarrow{k}_3} + \ldots\right)\right) \\
\frac{1}{\overrightarrow{k}_2}\left(1 + \frac{\overleftarrow{k}_1}{\overrightarrow{k}_3}\left(1 + \frac{\overleftarrow{k}_2}{\overrightarrow{k}_4} + \ldots\right)\right) \\
\frac{1}{\overrightarrow{k}_3}\left(1 + \frac{\overleftarrow{k}_2}{\overrightarrow{k}_4}\left(1 + \frac{\overleftarrow{k}_3}{\overrightarrow{k}_5} + \ldots\right)\right) \\
\vdots \\
\frac{1}{\overrightarrow{k_{n+1}}} + \frac{\overleftarrow{k}_n}{\overrightarrow{k_{n+1}}\Gamma_A} \\
\frac{1}{\Gamma_A}
\end{pmatrix} \tag{19}$$

The recursive form has a clear interpretation: $\overrightarrow{k_{i+1}}^{-1}$ is the residence time on site i before moving forward once; $r_{i+1}\overleftarrow{k}_i/\overrightarrow{k_{i+1}}$ is the contribution to the ith residence time from a particle that jumps to site i from $i+1$ before moving forward again. The mean first-passage time is the sum of the residence times, given by

DOI: 10.1021/acs.jpcc.8b08874
J. Phys. Chem. C 2019, 123, 1021−1031

$$\tau_m = \frac{1}{\vec{k}_1}\left(1 + \frac{\overleftarrow{k}_0 + \vec{k}_1}{\vec{k}_2}\left(1 + \frac{\overleftarrow{k}_1 + \vec{k}_2}{\vec{k}_3}(\ldots)\right)\right) \tag{20}$$

The recurrence relation for the residence time can also be seen from the flux condition: The population must leave to the right one more time than it enters from the left, $\vec{k}_i r_{i-1} - \overleftarrow{k}_{i-1} r_i = 1$.

3.2. SSTT. Following the discussion of Section 2.3, our objective is to solve the algebraic equation $\tilde{\mathbf{M}}\mathbf{p}^{ss} = \mathbf{p}_0$. We manage to reduce it as follows

$$\begin{pmatrix} 1 & 0 & & & & \\ & 1 & -\frac{\overleftarrow{k}_1}{q(1)} & & 0 & \\ & & 1 & -\frac{\overleftarrow{k}_2 q(1)}{q(2)} & & \\ & & & 1 & \ddots & \\ & & 0 & & \ddots & 1 & -\frac{\overleftarrow{k}_{n-1} q(n-2)}{q(n-1)} \\ & & & & & & 1 \end{pmatrix} \mathbf{p}^{ss} = \begin{pmatrix} 1 \\ \left(\frac{1}{\vec{k}_1} + \frac{\overleftarrow{k}_0}{\vec{k}_1 \vec{k}_2}\right)^{-1} \vec{k}_2^{-1} \\ \left(\frac{1}{\vec{k}_1} + \frac{\overleftarrow{k}_0}{\vec{k}_1 \vec{k}_2} + \frac{\overleftarrow{k}_0 \overleftarrow{k}_1}{\vec{k}_1 \vec{k}_2 \vec{k}_3}\right)^{-1} \vec{k}_3^{-1} \\ \vdots \\ \left(\frac{1}{\vec{k}_1} + \cdots + \frac{\prod_{i=0}^{n-1} \overleftarrow{k}_i}{\prod_{i=1}^{n+1} \vec{k}_i}\right)^{-1} \overrightarrow{k_{n+1}}^{-1} \\ \left(\frac{1}{\vec{k}_1} + \cdots + \frac{\prod_{i=0}^{n} \overleftarrow{k}_i}{\Gamma_A \prod_{i=1}^{n+1} \vec{k}_i}\right)^{-1} \Gamma_A^{-1} \end{pmatrix} \tag{21}$$

Here $q(1) = \vec{k}_2 + \overleftarrow{k}_0$, $q(2) = \vec{k}_2\vec{k}_3 + \vec{k}_3\overleftarrow{k}_0 + \overleftarrow{k}_0\overleftarrow{k}_1$, $q(3) = \overleftarrow{k}_2\overleftarrow{k}_0\overleftarrow{k}_1 + \vec{k}_4\vec{k}_2\vec{k}_3 + \vec{k}_4\vec{k}_3\overleftarrow{k}_0 + \vec{k}_4\overleftarrow{k}_0\overleftarrow{k}_1$, and so on. To generate these combinations, we define the sequence $s(x) = \{\vec{k}_2, \ldots, \overrightarrow{k_{x+1}}, \overleftarrow{k}_0, \overleftarrow{k}_1, \ldots, \overleftarrow{k_{x-1}}\}$; $q(x)$ is a sum of $x + 1$ products of nearest-neighbor elements in the sequence $s(x)$. For convenience, we use the notation $\overrightarrow{k_{n+2}} = \Gamma_A$.

The steady-state flux is given by $\Gamma_A p_{n+1}$, which can be found directly from the last row of eq 21. The other elements of the column vector on the right-hand side of eq 21 are the steady-state populations for chains that end with the site corresponding to that row.

In what follows, we exemplify our results for the MFPT and SSTT on several models; see Figures 1 and 2: (i) donor–bridge–acceptor configuration, where the bridge's energy is set constant and higher than the D and A levels; (ii) biased chain, representing a system under a constant electric field; and (iii) copolymer motifs, either alternating or stacked, representing

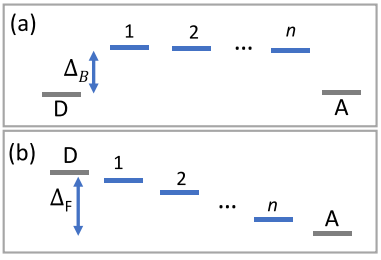

Figure 1. One-dimensional models: (a) Donor–bridge–acceptor chain with an energy gap (scaled by the temperature) Δ_B. (b) Biased system, exemplifying here a potential bias Δ_F toward the acceptor.

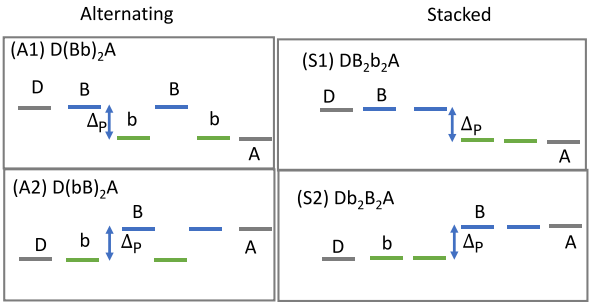

Figure 2. Examples of copolymer motifs. (A1,A2) Alternating chains with D connected to either the high- or low-energy monomers. (S1,S2) Stacked chains with D connected to either the high- or low-energy monomer. The D (A) sites are placed in resonance with the first (last) sites. There are even numbers of sites in the system in the presented examples. In the odd case, an additional site is added right before the acceptor site.

charge transport in quasi-1D chains such as motion along the pi stacking in a double-stranded DNA. Our results in these three cases assume that transitions are induced by a heat bath at thermal equilibrium; therefore, we enforce the detailed balance relation. We work with dimensionless energy parameters, scaled by temperature.

3.3. Example I: Donor–Bridge–Acceptor System. We consider here the ubiquitous donor–bridge–acceptor setup. We assume that bridge energies are uniform and that they are higher than both the donor and the acceptor levels; see Figure 1a. The MFPT is calculated from eq 18. Enforcing detailed balance, we set $\vec{k}_1 = e^{-\Delta_B}$, $\overleftarrow{k}_n = e^{-\Delta_B}$, and all other $\vec{k}_i$, $\overleftarrow{k}_i = 1$; n is the number of bridge sites, and Δ_B is the dimensionless energy gap between the donor/acceptor and the bridge (scaled by the temperature). The residence times are given by

$$\mathbf{r} = \begin{pmatrix} \frac{1}{\Gamma_A} + (n+1)e^{\Delta_B} \\ \frac{e^{-\Delta_B}}{\Gamma_A} + n \\ \frac{e^{-\Delta_B}}{\Gamma_A} + (n-1) \\ \frac{e^{-\Delta_B}}{\Gamma_A} + (n-2) \\ \vdots \\ \frac{e^{-\Delta_B}}{\Gamma_A} + 1 \\ \frac{1}{\Gamma_A} \end{pmatrix} \tag{22}$$

Summing them up while setting $\Gamma_A = 1$ for simplicity, we get

$$\tau_m = ne^{-\Delta_B} + (n+1)e^{\Delta_B} + \frac{1}{2}n^2 + \frac{1}{2}n + 2 \tag{23}$$

When $\Delta_B = 0$, this formula reduces to known results $\tau_m = (n+2)(n+3)/2$; see ref 24. In the opposite limit, when Δ_B is large, the linear term dominates eq 23, and it approaches the scaling $\tau_m \propto (n+1)e^{\Delta_B}$.

DOI: 10.1021/acs.jpcc.8b08874
J. Phys. Chem. C 2019, 123, 1021–1031

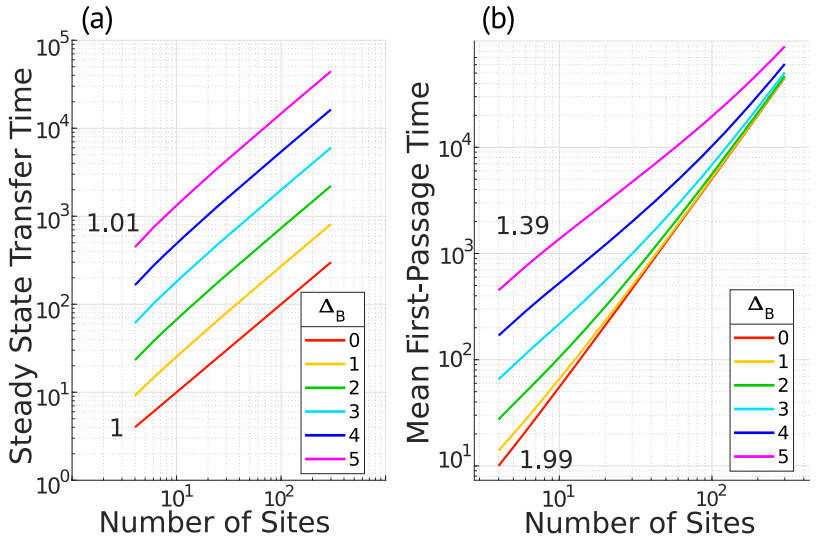

Figure 3. Dependence of (a) steady-state transfer time and (b) mean first-passage time on n for donor−bridge−acceptor systems.

The steady-state transfer time is derived from the last row of eq 21

$$k_{ss}^{-1} = \frac{1}{\overrightarrow{k_1}} + \ldots + \frac{\prod_{i=0}^{n} \overleftarrow{k_i}}{\prod_{i=1}^{n+1} \overrightarrow{k_i}} = e^{\Delta_B} + \ldots + e^{\Delta_B} + 1 \tag{24}$$

resulting in

$$\tau_{ss} = (n+1)e^{\Delta_B} + 1 \tag{25}$$

This measure is linear in n for all Δ_B. We therefore conclude that the MFPT and the SSTT agree so long as $\Delta_B \gg 1$. In this case, the bridge population is small, which agrees with our analysis of Section 2.4.

In Figure 3, we display the MFPT and the SSTT while increasing the system size and the bridge height Δ_B. The SSTT scales linearly with n, whereas the MFPT shows a transition from quadratic to linear scaling with the increase in Δ_B.

3.4. Example II: Biased Chain. We consider now a biased chain, as illustrated in Figure 1b. The system can be biased in opposite polarities, such that energies decrease or increase toward the acceptor. In what follows, we consider both cases, which we refer to as negative (decreasing) and positive (increasing) potential bias.

Negative Potential Bias, $E_D > E_A$. . The donor energy is placed above the acceptor, and the total gap is denoted by $\Delta_F \equiv |E_D - E_A|$. Recall that the chain comprises the donor, acceptor, and n intermediate states. For a nonincreasing potential bias, we get from eq 20 the MFPT

$$\tau_m = (n+2) + \sum_{i=0}^{n} \overleftarrow{k_i} + \sum_{i=1}^{n} (\overleftarrow{k_i}\overleftarrow{k_{i-1}}) + \sum_{i=2}^{n} (\overleftarrow{k_i}\overleftarrow{k_{i-1}}\overleftarrow{k_{i-2}}) + \ldots + (\overleftarrow{k_0}\overleftarrow{k_1}\ldots\overleftarrow{k_n}) \tag{26}$$

We now specifically assume a linear, constant gradient profile such that $\overleftarrow{k} = e^{-\Delta_F/(n+1)}$ and $\vec{k} = 1$. Using the analytical results of Sections 3.1 and 3.2, we find the MFPT

$$\tau_m = (n+2) + (n+1)e^{-\Delta_F/(n+1)} + ne^{-2\Delta_F/(n+1)} + (n-1)e^{-3\Delta_F/(n+1)} + \ldots + e^{-\Delta_F} \tag{27}$$

and the SSTT

$$\tau_{ss} = 1 + e^{-\Delta_F/(n+1)} + e^{-2\Delta_F/(n+1)} + \ldots + e^{-\Delta_F} \tag{28}$$

The MFPT is dominated by the $(n+2)$ term, whereas the SSTT is dominated by a constant (explicitly, by the Γ_A^{-1} rate constant) and the $e^{-\Delta_F/(n+1)}$ term. Therefore, by performing both transient and steady-state measurements, one can experimentally determine both the number of sites n and the potential drop Δ_F.

Positive Potential Bias, $E_D < E_A$. . When the potential energy linearly increases in the direction of the trap, the rate constants satisfy $\vec{k} = e^{-\Delta_F/(n+1)}$, $\overleftarrow{k} = 1$. Note that we define the gap by its magnitude, $\Delta_F = |E_A - E_D|$. The MFPT and the SSTT are

$$\tau_m = 1 + (n+2)e^{\Delta_F/(n+1)} + (n+1)e^{2\Delta_F/(n+1)} + \ldots + 2e^{\Delta_F} \tag{29}$$

and

$$\tau_{ss} = e^{\Delta_F/(n+1)} + e^{2\Delta_F/(n+1)} + \ldots + 2e^{\Delta_F} \tag{30}$$

As Δ_F grows, both mean first-passage time and steady-state transfer time approach $2e^{\Delta_F}$. This agreement is expected: When the forward energy gap is large, the steady-state populations on intermediate sites become small, and the time scales agree.

3.5. Example III: Copolymer Motifs. We consider polymers with two monomers, B and b of high energy (E_B) and low energy (E_b), with the scaled energy difference $\Delta_P = E_B - E_b$. The polymer may be alternating or stacked, for example, with sequences BbBbBb or BBBbbb, respectively. For simplicity, the donor (acceptor) is placed in resonance with the first (last) site. Examples of examined copolymers are presented in Figure 2. In what follows, we study the dependence of the MFPT and the SSTT on n, the number of intermediate sites, the parity of n, and Δ_P, the energy difference between monomers. Trends also depend on whether

DOI: 10.1021/acs.jpcc.8b08874
J. Phys. Chem. C 2019, 123, 1021−1031

Table 1. Alternating Polymer Motifs and Characteristic Transfer Times (Leading Terms in Bold)

	sequence	MFPT	SSTT
A1. (even)	$D(Bb)_mA$ $m = n/2$	$\mathbf{e^{\Delta_P}\left(\frac{1}{4}n^2 - \frac{1}{2}n\right)} + (n+2)e^{-\Delta_P} + \frac{1}{4}n^2 + 2n + 1$	$\mathbf{n} + 2e^{-\Delta_P}$
A2. (even)	$D(bB)_mA$ $m = n/2$	$\mathbf{e^{\Delta_P}\left(\frac{1}{4}n^2 + 2n + 1\right)} + \frac{1}{4}n^2 + \frac{1}{2}n + 2$	$\mathbf{e^{\Delta_P}(n+1)} + 1$
A3. (odd)	$D(Bb)_mBA$ $m = (n-1)/2$	$\mathbf{e^{\Delta_P}\left(\frac{1}{4}n^2 + \frac{1}{2}n - \frac{3}{4}\right)} + \frac{1}{4}n^2 + 2n + \frac{15}{4}$	$\mathbf{n} + 2$
A4. (odd)	$D(bB)_mbA$ $m = (n-1)/2$	$\mathbf{e^{\Delta_P}\left(\frac{1}{4}n^2 + n - \frac{5}{4}\right)} + (n-1)e^{-\Delta_P} + \frac{1}{4}n^2 + \frac{1}{2}n + \frac{21}{4}$	$\mathbf{e^{\Delta_P}(n-1)} + 3$

Table 2. Stacked Polymer Motifs and Characteristic Transfer Times (Leading Terms in Bold)

	sequence	MFPT	SSTT
S1. (even)	DB_mb_mA $m = n/2$	$\mathbf{\frac{1}{4}n^2} + \frac{3}{2}n + 2 + \left(\frac{1}{4}n^2 + n + 1\right)e^{-\Delta_P}$	$\mathbf{\frac{1}{2}n} + 1 + \left(\frac{1}{2}n + \frac{1}{2}\right)e^{-\Delta_P}$
S2. (even)	Db_mB_mA $m = n/2$	$\mathbf{e^{\Delta_P}\left(\frac{1}{4}n^2 + \frac{3}{2}n + 2\right)} + \frac{1}{4}n^2 + n + 1$	$\mathbf{e^{\Delta_P}\left(\frac{1}{2}n + 2\right)} + \frac{1}{2}n$
S3. (odd)	$DB_mb_{m+1}A$ $m = (n-1)/2$	$\mathbf{\frac{1}{4}n^2} + \frac{3}{2}n + \frac{9}{4} + \left(\frac{1}{4}n^2 + n + \frac{3}{4}\right)e^{-\Delta_P}$	$\mathbf{\frac{1}{2}n} + \frac{1}{2} + \left(\frac{1}{2}n + \frac{3}{2}\right)e^{-\Delta_P}$
S4. (odd)	$Db_mB_{m+1}A$ $m = (n-1)/2$	$\mathbf{e^{\Delta_P}\left(\frac{1}{4}n^2 + \frac{3}{2}n + \frac{5}{4}\right)} + \frac{1}{4}n^2 + n + \frac{7}{4}$	$\mathbf{e^{\Delta_P}\left(\frac{1}{2}n + \frac{5}{2}\right)} + \frac{1}{2}n - \frac{1}{2}$

the donor state is coupled to the high- or low-energy monomer. Our results are organized in Tables 1 and 2.

3.5.1. Alternating Polymers. Focusing first on the MFPT, we observe the following (see Table 1): (i) Polymers that end on the high-energy monomer (sequences A2 and A3, such as DbBbBbBA or DBbBbBA, respectively) show the functional form e^{Δ_P} but not $e^{-\Delta_P}$. This is because the residence times for low-energy monomers increase with e^{Δ_P}, whereas the residence time of the B monomer here does not depend on Δ_P. In contrast, polymers that end on the lower strand (DBbBbBbA or DbBbBbA) have both e^{Δ_P} and $e^{-\Delta_P}$ terms. In this case, high-energy monomers have residence times that depend on $e^{-\Delta_P}$, whereas low-energy monomers contribute the residence time e^{Δ_P}. (ii) For all four types of alternating chains, the MFPT scales as $n^2e^{\Delta_P}$. In contrast, the SSTT shows two different scaling laws, depending on whether the donor is in resonance with B or b. In the former case, $\tau_{ss} \propto n$, whereas in the latter case, the barrier energy shows up and $\tau_{ss} \propto ne^{\Delta_P}$.

3.5.2. Stacked Polymers. In this model, the copolymer is made of two halves of different content, which could correspond, for example, to different base pairings in DNA molecules; see refs 29 and 30. In this case, all rate constants $\vec{k}$, $\overleftarrow{k}$ are set equal to 1, besides a single rate where the monomers switch. For the mean first-passage time, this splits the sum of residence times into two groups: residence times corresponding to sites after the change in energy, which do not depend on Δ_P, and times corresponding to sites before the change in energy, which do manifest a Δ_P dependence. The results are quite natural; see Table 2: If we switch from high-energy sites toward low-energy sites as we move toward the acceptor, then we do not pay an energetic price and $\tau_m \propto n^2$, $\tau_{ss} \propto n$. In the opposite case, these times are increased by the e^{Δ_P} factor.

Overall, we find that: (i) The MFTT and SSTT of alternating configurations are typically longer than those for a stacked one. It is interesting to note that higher resistances were indeed measured for alternating DNA configurations, relative to stacked sequences,[29,30] in line with our calculations. Nevertheless, because coherent quantum effects are not included in this work, this agreement may be incidental. (ii) If n and Δ_P are large enough such that only the leading term matters, then it is generally possible to determine both Δ_P and n by jointly studying the steady-state lifetime and the mean first-passage time, assuming that we know the nature of the polymer (from the configurations S1−S4 and A1−A4) but not necessarily its length or energetics. First, we note that $\tau_m/\tau_{ss} \propto n$ in all cases, besides A1 and A3. In these special cases, the dominating term of steady-state lifetime is itself proportional to n. Also, all copolymers besides S1 and S3, show $\frac{1}{4}n^2e^{\Delta_P}$ as the leading term in the mean first-passage time. In all of these configurations, Δ_P can be readily determined once we find n.

4. OPTIMIZATION OF THE ENERGY PROFILE

Achieving a fast rate of charge transport through molecules is desirable for many applications. Experiments manifest an enhancement of hole transport in DNA by modifying the injection site, the sequence, and the chemical environment. These modifications alter the molecular energy profile and thus the driving force for charge migration.[31−33]

In this section, we ask the following question: Assuming fixed donor and acceptor site energies, what is the optimal energy profile for the intermediate n sites so as to minimize the transfer time and thus enhance the speed of transfer? We explore this question analytically and numerically for positive and negative biases. Central observations are that the MFPT and the SSTT are minimized under different principles and that the profile generally deviates from linearity and monotonicity. In Figure 4, we exemplify optimized setups under large bias, derived in the following discussion.

4.1. Negative Bias, $E_D > E_A$. *4.1.1. MFPT.* Let us first consider the negative bias case, with a total energy gap $\Delta_F = |E_D - E_A|$ between the donor and acceptor. As a

DOI: 10.1021/acs.jpcc.8b08874
J. Phys. Chem. C 2019, 123, 1021−1031

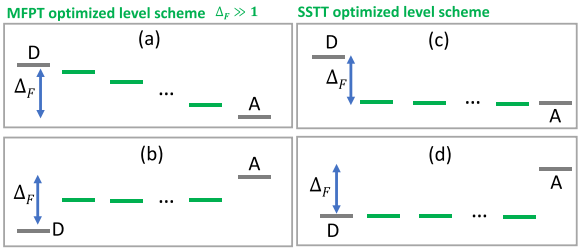

Figure 4. Illustrations of energy profiles that minimize the (a,b) MFPT and (c,d) SSTT under forward or reversed biases. The energy gap between the D and A sites is fixed. The position of the intermediate levels is determined by minimizing the transfer time. Under low bias (not shown), the energy profile minimizing the MFPT is nonmonotonic, and it generates an internal strong field, as we show in Figures 6 and 8

constraint, we demand that the energies of the sequence of n internal sites are nonincreasing. We assign a (temperature scaled) energy E_i to site i. The transition rate constant from site i to $i-1$ is set at $\overleftarrow{k_{i-1}} = e^{E_i - E_{i-1}}$ if $E_i < E_{i-1}$ and 1 otherwise. For simplicity, the trapping rate constant is taken as $\Gamma_A = 1$. Because the energies do not increase going toward the trap, all $\overrightarrow{k_i} = 1$, and the MFPT follows eq 26. The overall energy gap satisfies the constraint

$$\prod_{i=0}^{n} \overleftarrow{k_i} = e^{-\Delta_F} \tag{31}$$

The optimal rates in eq 26 fulfill the constraint and $n+1$ equations of the form

$$\begin{aligned}\frac{\partial \tau_m}{\partial \overleftarrow{k_i}} &= 1 + \overleftarrow{k_{i-1}} + \overleftarrow{k_{i+1}} + \overleftarrow{k_{i-2}}\overleftarrow{k_{i-1}} + \overleftarrow{k_{i-1}}\overleftarrow{k_{i+1}} + \overleftarrow{k_{i+1}}\overleftarrow{k_{i+2}} \\ &\quad \ldots + \overleftarrow{k_0}\overleftarrow{k_1} \ldots \overleftarrow{k_{i-1}}\overleftarrow{k_{i+1}} \ldots \overleftarrow{k_n} \\ &= \lambda \overleftarrow{k_0}\overleftarrow{k_1} \ldots \overleftarrow{k_{i-1}}\overleftarrow{k_{i+1}} \ldots \overleftarrow{k_n}\end{aligned} \tag{32}$$

where the constant λ is the Lagrange multiplier; $\overleftarrow{k_j} = 0$ if $j < 0$. As an example, let us consider the case with two intermediate sites, $n = 2$. The MFPT is

$$\tau_m = 4 + \overleftarrow{k_0} + \overleftarrow{k_1} + \overleftarrow{k_2} + \overleftarrow{k_0}\overleftarrow{k_1} + \overleftarrow{k_1}\overleftarrow{k_2} + \overleftarrow{k_0}\overleftarrow{k_1}\overleftarrow{k_2} \tag{33}$$

and the following four equations should be jointly solved

$$1 + \overleftarrow{k_1} + \overleftarrow{k_1}\overleftarrow{k_2} = \lambda \overleftarrow{k_1}\overleftarrow{k_2} \tag{34a}$$

$$1 + \overleftarrow{k_0} + \overleftarrow{k_2} + \overleftarrow{k_0}\overleftarrow{k_2} = \lambda \overleftarrow{k_0}\overleftarrow{k_2} \tag{34b}$$

$$1 + \overleftarrow{k_1} + \overleftarrow{k_0}\overleftarrow{k_1} = \lambda \overleftarrow{k_0}\overleftarrow{k_1} \tag{34c}$$

$$\overleftarrow{k_0}\overleftarrow{k_1}\overleftarrow{k_2} = e^{-\Delta_F} \tag{34d}$$

From symmetry, note that the first and last transition rates are identical, $\overleftarrow{k_2} = \overleftarrow{k_0}$. In general, because eq 32 is symmetric with respect to replacing each $\overleftarrow{k_i}$ with $\overleftarrow{k_{n-i}}$, pairs of rate constants of equal distance from the first and last sites will be identical. For $n = 2$, the minimization problem involves solving a third-degree polynomial in $\sqrt{\lambda}$

$$0 = \lambda\sqrt{\lambda} - 2\lambda + \sqrt{\lambda} - e^{\Delta_F} \tag{35}$$

where

$$\overleftarrow{k_0} = \overleftarrow{k_2} = \frac{1}{\sqrt{\lambda} - 1}, \quad \overleftarrow{k_1} = \frac{1}{\sqrt{\lambda}} \tag{36}$$

We can also organize eq 35 as $x(x-1)^2 = e^{\Delta_F}$ with $x = \sqrt{\lambda}$. As expected, when Δ_F becomes large, x grows and approaches $x \approx e^{\Delta_F/3}$, which corresponds to constant spacing (linear profile). Optimization of the model with n intermediate sites requires solving a similar $n+1$-degree polynomial.

The analytic calculation above constrains the energies to be nonincreasing. This constraint is not enforced in simulations that, in fact, reveal situations in which the transfer times are minimized with nonmonotonic profiles. In Figures 5 and 6 we demonstrate such calculations using gradient descent. We find that when n is small and Δ_F is large, starting from the D, the energies descend slowly (small local bias), then more quickly toward the center (large local bias), and again slowly at the end of the chain. In contrast, when n is large and Δ_F small, the first internal site is placed *above* the donor state. The rest of the sites descend linearly, reaching below the acceptor state; see Figure 6a,b. This result can be rationalized as follows: The system pays the cost of a large energy jump in the first transition (slow-down of transfer), yet this early barrier prevents the carrier from going backward toward the donor from the internal sites. Nevertheless, if we force the internal sites to take values only in between the donor and acceptor levels, then we obtain profiles that are similar to the small-n large-Δ_F case.

Nonmonotonic internal profiles allow fast transfer when the external bias Δ_F is small relative to the temperature. In such low-field cases, the levels organize to create a large internal field, opposing thermal fluctuations and facilitating fast

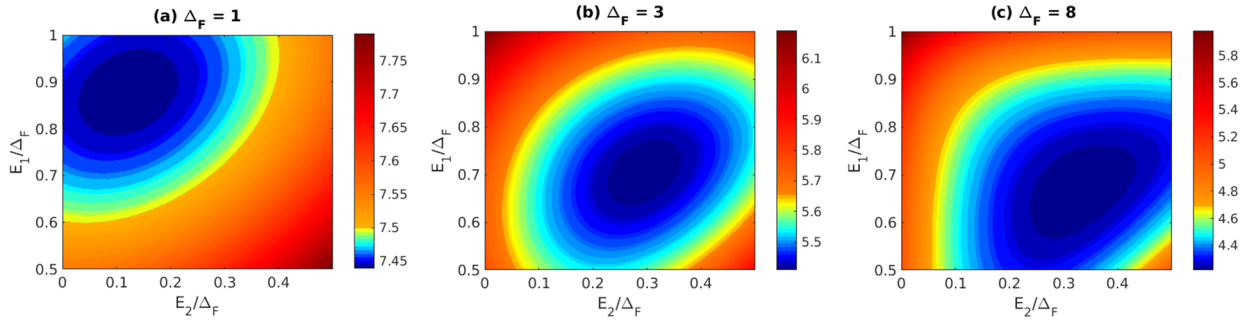

Figure 5. Simulations of the mean first-passage time for configurations with two internal sites (D, 1, 2, A) for negative bias, $E_D > E_A$. As Δ_F increases, the optimal configuration (minimum MFPT) approaches the profile $\left(\frac{2}{3}\Delta_F, \frac{1}{3}\Delta_F\right)$.

DOI: 10.1021/acs.jpcc.8b08874
J. Phys. Chem. C 2019, 123, 1021−1031

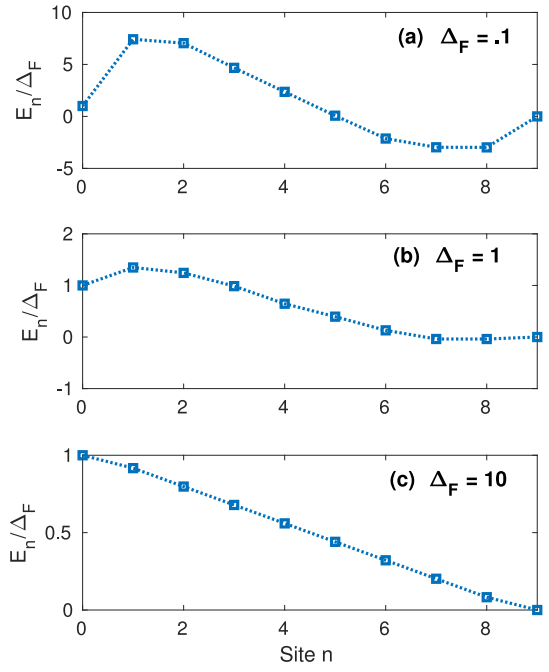

Figure 6. Negative bias, $E_D > E_A$. Energy profile obtained numerically using gradient descent by minimizing the MFPT for systems with eight internal sites (D, 1, ..., 8, A).

transport. This principle could be used in the design of biomolecules that support fast charge migration.[33]

4.1.2. SSTT. Continuing with the same model, with a nonincreasing profile, we turn to the steady-state transfer time

$$\tau_{ss} = \overleftarrow{k_0} + \overleftarrow{k_0}\overleftarrow{k_1} + \overleftarrow{k_0}\overleftarrow{k_1}\overleftarrow{k_2} + \ldots + \prod_0^n \overleftarrow{k_i} \tag{37}$$

This expression is minimized when $\overleftarrow{k_0} = e^{-\Delta_F}$, $\overleftarrow{k_i} = 1$ for $i \neq 0$, resulting in the minimum steady-state transfer time of $(n + 1)e^{-\Delta_F}$. In other words, the fastest process occurs when all of the internal sites are aligned with the acceptor; that is, the energy jump occurs immediately, from the donor to the first site, $n = 1$.

4.2. Positive Bias, $E_D < E_A$. *4.2.1. MFPT.* We now consider a low-energy donor, n nondecreasing energy levels, and a high-energy acceptor site. We define the gap as $\Delta_F = |E_D - E_A|$. This arrangement implies that $\overleftarrow{k} = 1$, whereas the forward rates are to be optimized. The MFPT is

$$\tau_m = \left(\frac{1}{\Gamma_A} + \frac{1}{\overrightarrow{k_{n+1}}} + \ldots + \frac{1}{\overrightarrow{k_1}}\right) + \left(\frac{1}{\Gamma_A \overrightarrow{k_{n+1}}} + \frac{1}{\overrightarrow{k_{n+1}}\overrightarrow{k_n}} + \ldots + \frac{1}{\overrightarrow{k_2}\overrightarrow{k_1}}\right) + \ldots + \frac{1}{\Gamma_A \prod_{i=1}^{n+1} \overrightarrow{k_i}} \tag{38}$$

For simplicity, taking $\Gamma_A = 1$, we get

$$\tau_m = \left(\frac{2}{\overrightarrow{k_{n+1}}} + \frac{1}{\overrightarrow{k_n}} \ldots + \frac{1}{\overrightarrow{k_1}}\right) + \left(\frac{2}{\overrightarrow{k_{n+1}}\overrightarrow{k_n}} + \frac{1}{\overrightarrow{k_n}\overrightarrow{k_{n-1}}} + \ldots + \frac{1}{\overrightarrow{k_2}\overrightarrow{k_1}}\right) + \ldots + \frac{2}{\prod_{i=1}^{n+1} \overrightarrow{k_i}} + 1 \tag{39}$$

Minimizing the MFPT subjected to the constraint $\prod_{i=1}^{n+1} \overrightarrow{k_i} = e^{-\Delta_F}$, the equations have no convenient symmetries. For example, $n = 1$ yields

$$\tau_m = 1 + \frac{1}{\overrightarrow{k_1}} + \frac{2}{\overrightarrow{k_2}} + \frac{2}{\overrightarrow{k_1}\overrightarrow{k_2}} \tag{40}$$

Whereas this equation can be readily minimized with the constraint, we proceed with the general formalism of Lagrange multipliers and solve the system

$$-\frac{1}{\overrightarrow{k_1}^2} - \frac{2}{\overrightarrow{k_1}^2\overrightarrow{k_2}} = \lambda \overrightarrow{k_2} \tag{41a}$$

$$-\frac{2}{\overrightarrow{k_2}^2} - \frac{2}{\overrightarrow{k_1}\overrightarrow{k_2}^2} = \lambda \overrightarrow{k_1} \tag{41b}$$

$$\overrightarrow{k_1}\overrightarrow{k_2} = e^{-\Delta_F} \tag{41c}$$

This problem can be solved by noting that

$$-\frac{1}{\overrightarrow{k_1}^2\overrightarrow{k_2}} - \frac{2}{\overrightarrow{k_1}^2\overrightarrow{k_2}^2} = \lambda = -\frac{2}{\overrightarrow{k_1}\overrightarrow{k_2}^2} - \frac{2}{\overrightarrow{k_1}^2\overrightarrow{k_2}^2} \tag{42}$$

which implies that $\overrightarrow{k_2} = 2\overrightarrow{k_1}$, or explicitly

$$\overrightarrow{k_1} = e^{1/2(-\ln 2 - \Delta_F)}, \quad \overrightarrow{k_2} = e^{1/2(\ln 2 - \Delta_F)} \tag{43}$$

Figures 7 and 8 present simulation results, where we allowed the internal potential profile to become nonmonotonic (unlike the analytic derivation). We find that for large n and large Δ_F, the internal sites cluster at a level slightly above the midgap between the donor and acceptor. In contrast, for very small Δ_F,

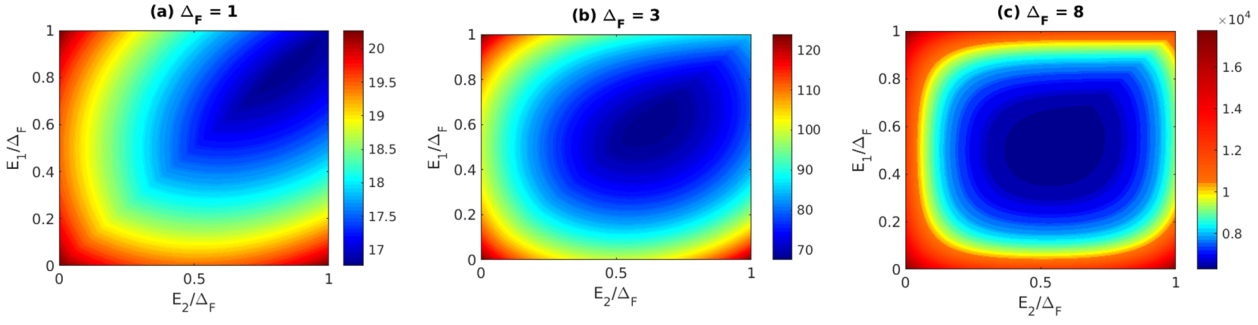

Figure 7. Simulations of the mean first-passage time for a two-state system with $E_D < E_A$. As the gap Δ_F increases, the optimal configuration is of two states placed together at around $\Delta_F/2$.

DOI: 10.1021/acs.jpcc.8b08874
J. Phys. Chem. C 2019, 123, 1021−1031

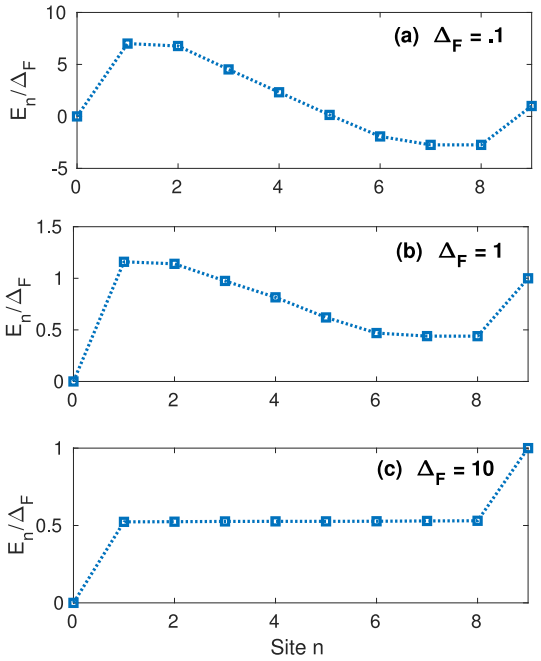

Figure 8. Energy profile obtained numerically by minimizing the MFPT for a system with eight intermediate sites under a positive bias $E_D < E_A$. At small Δ_F, the profiles under positive and negative biases look identical. Compare panel a to Figure 6a.

the energy profile first increases, thus artificially creating a large internal field, which facilities fast transfer. In fact, when Δ_F is small, the results for positive and negative biases are very similar; compare Figures 6a and 8a.

4.2.2. SSTT. We calculate the SSTT using eq 21, now assuming a nondecreasing profile

$$\tau_{ss} = \left[\overrightarrow{k}_1^{-1} + (\overrightarrow{k}_1\overrightarrow{k}_2)^{-1} + \ldots + \prod_{i=1}^{n+1}\overrightarrow{k}_i^{-1}\right] \tag{44}$$

The minimum MFPT, subject to the constraint $\prod_{i=1}^{n+1} = e^{-\Delta_F}$, can be intuitively obtained: Each term in eq 44 is greater than or equal to the preceding term. Therefore, τ_{ss} is minimized once we take $\overrightarrow{k_{n+1}} = e^{-\Delta_F}$ and $\overrightarrow{k_i} = 1$ for all $i \neq n+1$. This setup is illustrated in Figure 4d: Besides the last site, all sites align with the donor state.

4.3. Principles for Optimization of Transfer Time. Given fixed donor and acceptor site energies, what is the optimal energy level profile for the intermediate sites (one that would support the fastest transport)? It is fascinating to note that the answer dramatically differs for the different measures. On the basis of the analytical results and simulations of Sections 4.1 and 4.2, we organize the following guidelines:

(i) The MFPT is minimized by prohibiting homecoming to the donor site. For a negative bias problem, $E_D > E_A$, a linearly decaying profile minimizes the MFPT when the donor–acceptor gap is large. However, when the gap is small, an internal bias develops, suppressing the restoration of the donor population; see Figure 6. Similarly, at small positive bias $E_D \lesssim E_A$, an internal negative profile develops, assisting particles in sliding forward; see Figure 8b. When $E_A \gg E_D$, the optimal profile is flat about half way between D and A. In this case, energetically costly jumps occur at the boundaries, but the particle diffuses without barriers through the bulk of the system.

(ii) The SSTT is minimized when populations along the system are high. The rationale here is that k_{ss} is proportional to the acceptor's population, and thus high occupations throughout all sites carry on to a high population at the acceptor site. Thus when $E_D > E_A$, highest occupations are achieved when all internal sites are aligned with the acceptor; that is, the energy jump occurs immediately, from the donor to the first site, $n = 1$. Along the same principle, when $E_D < E_A$, we minimize the steady state transfer time when all sites align with the donor site, maintaining a high population throughout.

5. SUMMARY

Using kinetic equations, we studied particle transfer in 1D systems with different motifs: linear, branched, uniform, biased, homogeneous, and multicomponent systems. The central results of our work are as follows: (i) We derived an intuitive relationship between the MFPT and the SSTT, eq 14. (ii) We obtained closed-form expressions for the MFPT and the SSTT in nearest-neighbor 1D chains. (iii) We exemplified our results on experimentally relevant setups, such as donor–bridge–acceptor systems, biased chains, and stacked and alternating copolymers and discussed the physical information that can be gained from the MFPT and the SSTT. (iv) We minimized the transit time through chains by optimizing the energy profile. Here we found that the MFPT and the SSTT were minimized under fundamentally different design rules. Most strikingly, under shallow external potentials of the order of the thermal energy, $\Delta_F \leq 1$, the system achieved fast transit time if the levels were set so as to create a strong internal field.

This work clarifies on the relationship between transient and steady-state measures in classical kinetic networks. This incoherent hopping dynamics can also emerge in quantum dissipative systems under several assumptions such as weak system-bath coupling, Markovian baths, and fast decoherence rates. It is worthwhile to mention studies of the MFPT in complex scale-invariant media[34] and in the context of enzymatic chemical reactions in biochemistry.[35,36] Nevertheless, in these works, the networks included loops, a motif that was not investigated in the present study.

Beyond the analysis of the MFPT, a rigorous general machinery, as described in ref 37, provides the probability distribution function of passage time, which contains information on higher cumulants. However, because our focus has been on developing a relationship between the SSTT and the MFPT, we elected to use more elementary tools.

It is also interesting to consider extensions of this work, particularly the enhancement of the transfer speed, to systems under thermal gradients.[38] The analysis of transfer processes in networks beyond 1D and the role of quantum coherent effects in corresponding quantum systems[39] will be the focus of future work.

■ ASSOCIATED CONTENT

Supporting Information

The Supporting Information is available free of charge on the ACS Publications website at DOI: 10.1021/acs.jpcc.8b08874.

S1: Setting the steady-state problem. S2: Derivation of the MFPT for graphs with multiple acceptors (PDF)

■ AUTHOR INFORMATION

Corresponding Author

*E-mail: dvira.segal@utoronto.ca.

DOI: 10.1021/acs.jpcc.8b08874
J. Phys. Chem. C 2019, 123, 1021−1031

ORCID

Dvira Segal: 0000-0002-8027-8920

Notes

The authors declare no competing financial interest.

■ ACKNOWLEDGMENTS

D.S. acknowledges the Natural Sciences and Engineering Research Council (NSERC) of Canada Discovery Grant and the Canada Chair Program. N.K. was supported by the NSERC Undergraduate Student Research Award (USRA) program. We thank the anonymous reviewers for valuable comments.

■ REFERENCES

(1) May, V.; Kühn, E. *Charge and Energy Transfer Dynamics in Molecular Systems*; Wiley-VCH: Berlin, 2011.
(2) Van Kampen, N. G. *Stochastic Processes in Physics and Chemistry*; Elsevier: Amsterdam, The Netherlands, 1992.
(3) Iyer-Biswas, S.; Zilman, A. First-Passage Processes in Cellular Biology. *Adv. Chem. Phys.* **2016**, *160*, 261−306.
(4) Bar-Haim, A.; Klafter, J. On Mean residence and First-Passage Times in Finite One-Dimensional Systems. *J. Chem. Phys.* **1998**, *109*, 5187−5193.
(5) Lewis, F. D.; Wu, T.; Liu, X.; Letsinger, R. L.; Greenfield, S. R.; Miller, S. E.; Wasielewski, M. R. Dynamics of Photoinduced Charge Separation and Charge Recombination in Synthetic DNA Hairpins with Stilbenedicarboxamide Linkers. *J. Am. Chem. Soc.* **2000**, *122*, 2889−2902.
(6) Lewis, F. D.; Letsinger, R. L.; Wasielewski, M. R. Dynamics of Photoinduced Charge Transfer and Hole Transport in Synthetic DNA Hairpins. *Acc. Chem. Res.* **2001**, *34*, 159−170.
(7) Lin, S.-H.; Fujitsuka, M.; Majima, T. Dynamics of Excess-Electron Transfer through Alternating Adenine:Thymine Sequences in DNA. *Chem. - Eur. J.* **2015**, *21*, 16190−16194.
(8) Wierzbinski, E.; Venkatramani, R.; Davis, K. L.; Bezer, S.; Kong, J.; Xing, Y.; Borguet, E.; Achim, C.; Beratan, D. N.; Waldeck, D. H. The Single-Molecule Conductance and Electrochemical Electron-Transfer Rate Are Related by a Power Law. *ACS Nano* **2013**, *7*, 5391−5401.
(9) Wang, L.; Wang, L.; Zhang, L.; Xiang, D. Advance of Mechanically Controllable Break Junction for Molecular Electronics. *Top. Curr. Chem. (Z)* **2017**, *375* (3), 1−42.
(10) Levine, I.; Gupta, S.; Bera, A.; Ceratti, D.; Hodes, G.; Cahen, D.; Guo, D.; Savenije, T. J.; Avila, J.; Bolink, H. J. Can We Use Time-Resolved Measurements to Get Steady-State Transport Data for Halide Perovskites. 2018, arXiv:1805.00263 [physics.app-ph]. arXiv.org e-Print archive. https://arxiv.org/abs/1805.00263.
(11) Nitzan, A. A. Relationship between Electron-Transfer Rates and Molecular Conduction. *J. Phys. Chem. A* **2001**, *105* (12), 2677−2679.
(12) Nitzan, A. The Relationship Between Electron Transfer Rate and Molecular Conduction 2. The Sequential Hopping Case. *Isr. J. Chem.* **2002**, *42*, 163−166.
(13) Berlin, Y. A.; Ratner, M. A. Intra-Molecular Electron Transfer and Electric Conductance via Sequential Hopping: Unified Theoretical Description. *Radiat. Phys. Chem.* **2005**, *74*, 124−131.
(14) Traub, N. C.; Brunschwig, B. S.; Lewis, N. S. Relationships between Nonadiabatic Bridged Intramolecular, Electrochemical, and Electrical Electron-Transfer Processes. *J. Phys. Chem. B* **2007**, *111*, 6676−6683.
(15) Venkatramani, R.; Wierzbinski, E.; Waldeck, D. H.; Beratan, D. N. Breaking the Simple Proportionality between Molecular Conductances and Charge Transfer Rates. *Faraday Discuss.* **2014**, *174*, 57−78.
(16) Zhou, X.-S.; Liu, L.; Fortgang, P.; Lefevre, A.-S.; Serra-Muns, A.; Raouafi, N.; Amatore, C.; Mao, B.-W.; Maisonhaute, E.; Schöllhorn, B. Do Molecular Conductances Correlate with Electrochemical Rate Constants? Experimental Insights. *J. Am. Chem. Soc.* **2011**, *133*, 7509−7516.
(17) Bueno, P. R. Common Principles of Molecular Electronics and Nanoscale Electrochemistry. *Anal. Chem.* **2018**, *90*, 7095−7106.
(18) Bixon, M.; Giese, B.; Wessely, S.; Langenbacher, T.; Michel-Beyerle, M. E.; Jortner, J. Long-Range Charge Hopping in DNA. *Proc. Natl. Acad. Sci. U. S. A.* **1999**, *96* (21), 11713−11716.
(19) Giese, B. Long Distance Charge Transport in DNA: The Hopping Mechanism. *Acc. Chem. Res.* **2000**, *33* (9), 631−636.
(20) Berlin, Y. A.; Burin, A. L.; Ratner, M. A. Charge Hopping in DNA. *J. Am. Chem. Soc.* **2001**, *123*, 260−268.
(21) Blaustein, G. S.; Lewis, F. D.; Burin, A. L. Kinetics of Charge Separation in Poly(A)-Poly(T) DNA Hairpins. *J. Phys. Chem. B* **2010**, *114*, 6732.
(22) Livshits, G. I.; Stern, A.; Rotem, D.; Borovok, N.; Eidelshtein, G.; Migliore, A.; Penzo, E.; Wind, S. J.; Di Felice, R.; Skourtis, S. S.; et al. Long-Range Charge Transport in Single G-Quadruplex DNA Molecules. *Nat. Nanotechnol.* **2014**, *9*, 1040−1046.
(23) Jimenez-Monroy, K. L.; Renaud, N.; Drijkoningen, J.; Cortens, D.; Schouteden, K.; van Haesendonck, C.; Guedens, W. J.; Manca, J. V.; Siebbeles, L. D. A.; Grozema, F. C.; et al. High Electronic Conductance through Double-Helix DNA Molecules with Fullerene Anchoring Groups. *J. Phys. Chem. A* **2017**, *121*, 1182−1188.
(24) Polizzi, N. F.; Therien, M. J.; Beratan, D. N. Mean First-Passage Times in Biology. *Isr. J. Chem.* **2016**, *56*, 816−824.
(25) Polizzi, N. F.; Skourtis, S. S.; Beratan, D. N. Physical Constraints on Charge Transport through Bacterial Nanowires. *Faraday Discuss.* **2012**, *155*, 43−62.
(26) Carmeli, B.; Nitzan, A. First-Passage Times and the Kinetics of Unimolecular Dissociation. *J. Chem. Phys.* **1982**, *76*, 5321−5333.
(27) Segal, D.; Nitzan, A.; Davis, W. B.; Wasielewski, M. R.; Ratner, M. A. Electron Transfer Rates in Bridged Molecular Systems: A Steady State Analysis of Coherent Tunneling and Thermal Transitions. *J. Phys. Chem. B* **2000**, *104*, 3817−3829.
(28) Conte, S. D.; deBoor, C. *Elementary Numerical Analysis*; McGraw-Hill: New York, 1972.
(29) Xiang, L.; Palma, J. L.; Bruot, C.; Mujica, V.; Ratner, M. A.; Tao, N. Intermediate Tunneling-Hopping Regime in DNA Charge Transport. *Nat. Chem.* **2015**, *7*, 221−226.
(30) Liu, C.; Xiang, L.; Zhang, Y.; Zhang, P.; Beratan, D. N.; Li, Y.; Tao, N. Engineering Nanometer-Scale Coherence in Soft Matter. *Nat. Chem.* **2016**, *8*, 941−945.
(31) Thazhathveetil, A. K.; Trifonov, A.; Wasielewski, M. R.; Lewis, F. D. Increasing the Speed Limit for Hole Transport in DNA. *J. Am. Chem. Soc.* **2011**, *133* (30), 11485−11487.
(32) Mishra, A. K.; Young, R. M.; Wasielewski, M. R.; Lewis, F. D. Wirelike Charge Transport Dynamics for DNA-Lipid Complexes in Chloroform. *J. Am. Chem. Soc.* **2014**, *136* (44), 15792−15797.
(33) Renaud, N.; Harris, M. A.; Singh, A. P. N.; Berlin, Y. A.; Ratner, M. A.; Wasielewski, M. R.; Lewis, F. D.; Grozema, F. C. Deep-Hole Transfer Leads to Ultrafast Charge Migration in DNA Hairpins. *Nat. Chem.* **2016**, *8*, 1015−1021.
(34) Condamin, S.; Bénichou, O.; Tejedor, V.; Voituriez, R.; Klafter, J. First-Passage Times in Complex Scale-Invariant Media. *Nature (London, U. K.)* **2007**, *450*, 77−80.
(35) Schmiedl, T.; Seifert, U. Stochastic Thermodynamics of Chemical Reaction Networks. *J. Chem. Phys.* **2007**, *126*, 044101.
(36) Cao, J. Michaelis-Menten Equation and Detailed Balance in Enzymatic Networks. *J. Phys. Chem. B* **2011**, *115*, 5493−5498.
(37) Cao, J.; Silbey, R. J. Generic Schemes for Single-Molecule Kinetics. 1: Self-Consistent Pathway Solutions for Renewal Processes. *J. Phys. Chem. B* **2008**, *112*, 12867−12880.
(38) Craven, G. T.; Nitzan, A. Electron Transfer Across a Thermal Gradient. *Proc. Natl. Acad. Sci. U. S. A.* **2016**, *113*, 9421−9429.
(39) Cao, J.; Silbey, R. J. Optimization of Exciton Trapping in Energy Transfer Processes. *J. Phys. Chem. A* **2009**, *113*, 13825−13838.

DOI: 10.1021/acs.jpcc.8b08874
J. Phys. Chem. C 2019, 123, 1021−1031